Chapter 3

Optical Turbulence in the Atmosphere

Overview: In this chapter we present a brief treatment of atmospheric turbulence as it pertains to *velocity fluctuations* (classical turbulence), *temperature fluctuations*, and *index of refraction fluctuations*, the latter often referred to as *optical turbulence.* The primary objective here is to introduce various models of the *power spectrum for optical turbulence* that are commonly used in optical wave propagation studies. These models include the *Kolmogorov power-law spectrum, Tatarskii spectrum* (with inner scale parameter), *von Kármán spectrum* (with both inner scale and outer scale parameters), and the *modified atmospheric spectrum* (with both inner scale and outer scale parameters). However, only the modified atmospheric spectrum features a high wave number "bump" just prior to the onset of the dissipation range that has been observed in temperature data. It has been shown that the presence of this spectral bump in the temperature spectrum induces a corresponding bump in the refractive-index spectrum that can have important consequences on various aspects of optical wave propagation through the atmosphere, particularly in regards to scintillation.

In the last section of the chapter we discuss the notion of *temporal statistics* for the atmosphere. Here we rely on *Taylor's hypothesis of frozen turbulence* to convert spatial statistics to temporal statistics based on the transverse wind speed. We use this same idea in later chapters to convert spatial statistics concerning beam wave propagation to corresponding temporal statistics. In this latter case, the shape of the phase front radius of curvature of the optical wave must also be taken into account.

3.1 Introduction

Classical studies of turbulence were concerned with fluctuations in the velocity field of a viscous fluid. In particular, it was observed that the longitudinal wind velocity associated with the turbulent atmosphere fluctuates randomly about its mean value. That is, the wind velocity field assumes the nature of a *random* or *stochastic field*, which means that at each point in space and time within the flow the velocity may be represented by a random variable.

Turbulent motion of the atmosphere in the presence of moisture and temperature gradients gives rise to disturbances in the atmosphere's refractive index in the form of cells called optical turbules. Early studies by Kolmogorov [1] suggest that a subclass of all optical turbules has a degree of statistical consistency that permits a meaningful theoretical treatment. We define *optical turbulence* as the fluctuations in the index of refraction resulting from small temperature fluctuations. Random space-time redistribution of the refractive index causes a variety of effects on an optical wave related to its temporal irradiance fluctuations (scintillation) and phase fluctuations.

A statistical approach has been fruitful over the years in describing both atmospheric turbulence and its various effects on optical/IR systems. For the purpose of mathematical simplification, it is often necessary in such statistical approaches to assume that point separations within certain scale sizes exhibit the important characteristics of statistical homogeneity and isotropy studied in Chap. 2. In general, *statistical homogeneity* of the random field implies that the mean value of the field is constant and that correlations between random fluctuations in the field from point to point are independent of the chosen observation points, depending only on their vector separation. Moreover, if the random fluctuations are also *statistically isotropic*, then point-to-point correlations depend only on the magnitude of the vector separation between observation points. In this chapter we discuss random fluctuations associated with the *velocity, temperature*, and *index of refraction* of the atmosphere within the framework developed in Chap. 2.

3.2 Kolmogorov Theory of Turbulence

Considering the atmosphere as a viscous fluid, experience has dictated that it has two distinct states of motion—laminar and turbulent. The distinction between these states lies in the fact that mixing does not occur in *laminar flow* for which

the velocity flow characteristics are uniform or change in some regular fashion. In *turbulent flow*, the velocity field loses its uniform characteristics due to dynamic mixing and acquires random subflows called *turbulent eddies*.

In the earliest study of turbulent flow, Reynolds used similarity theory to define a nondimensional quantity $\mathrm{Re} = Vl/\nu$, now called the *Reynolds number*. Here, V and l are the characteristic velocity (speed) and dimension of the flow (in units of m/s and m, respectively) and ν is the kinematic viscosity (in units of m^2/s). The transition from laminar flow to turbulent motion takes place at a *critical Reynolds number*, above which the motion is considered turbulent. Close to the ground the characteristic scale size is $l \sim 2$ m, characteristic wind speed is 1 to 5 m/s, and $\nu \sim 0.15 \times 10^{-4}$ m^2/s, leading to large Reynolds numbers on the order $\mathrm{Re} \sim 10^5$. In such cases the motion is considered highly turbulent.

Turbulence is fundamentally a nonlinear process as described by the governing Navier-Stokes equations. Because of mathematical difficulties in solving these equations, Kolmogorov [1] developed a statistical theory of turbulence that relies heavily on dimensional analysis and additional simplifications and approximations. Thus, turbulence theory as we know it today is not derived from first principles.

3.2.1 Velocity fluctuations

The classical theory of turbulence as developed in the early 1940s by Kolmogorov concerns random fluctuations in both the magnitude and direction of the velocity field of a fluid. His theory was presented in terms of a set of hypotheses, based heavily on physical insight. For sufficiently large Reynolds numbers, it was hypothesized that the small-scale structure of turbulence is statistically homogeneous, isotropic, and independent of the large-scale structure, and further, that the motion associated with the small-scale structure is uniquely determined by the kinematic viscosity ν and the average rate of dissipation ε (in units of $\mathrm{m}^2/\mathrm{s}^3$) of the turbulent energy per unit mass of the fluid.

To understand the structure of atmospheric turbulence, it is convenient to adopt a visualization tool called the *energy cascade theory* of turbulence due to Richardson [2] (see Fig. 3.1). The source of energy at large scales is either wind shear or convection. Under the cascade theory, the wind velocity increases until it reaches a point at which the critical Reynolds number is exceeded. This action creates local unstable air masses (conceptualized as "eddies") with characteristic dimensions slightly smaller than, and independent of, the parent flow. Under the influence of inertial forces, the larger eddies break up into smaller eddies to form a continuum of eddy size for the transfer of energy from a macroscale L_0 (called the *outer scale of turbulence*) to a microscale l_0 (called the *inner scale of turbulence*). The family of eddies bounded above by the outer scale L_0 and below by the inner scale l_0 forms the *inertial subrange*. Scale sizes smaller than the inner scale l_0 belong to the *viscous dissipation rang*e. In this last regime, the turbulent eddies disappear and the remaining energy in the fluid motion is dissipated as heat.

The outer scale L_0 denotes the scale size below which turbule properties are independent of the parent flow. In the surface layer up to $\sim$100 m, the outer scale L_0 is

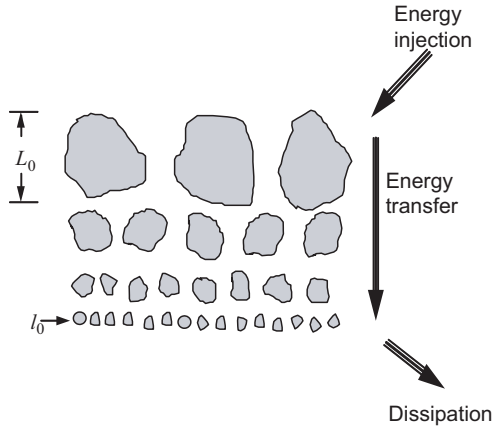

Figure 3.1 Kolmogorov cascade theory of turbulence, where L_0 denotes the outer scale and l_0 is the inner scale. Eddies between scale sizes l_0 and L_0 form the inertial subrange.

usually assumed to grow linearly with the order of the height above ground of the observation point [3,4]. Eddies of scale sizes smaller than L_0 are assumed *statistically homogeneous* and *isotropic*, whereas those equal to or larger than L_0 are generally *nonisotropic* and their structure is not well defined. Above 100 m, the horizontal dimension of L_0 is generally much greater than its vertical dimension because of stratification. As the turbulent eddies become smaller and smaller, the relative amount of energy dissipated by viscous forces increases until the energy dissipated matches that supplied by the kinetic energy of the parent flow. When this happens, the Reynolds number is reduced to the order of unity and the associated eddy size then defines the inner scale of turbulence l_0. The inner scale is typically on the order of 1 to 10 mm near the ground, but is on the order of centimeters or more in the troposphere and stratosphere.

By using dimensional analysis, Kolmogorov showed that the longitudinal structure function of wind velocity (parallel to the vector **R** connecting two observation points) in the inertial range satisfies the universal $2/3$ power law

$$D_{RR}(R) = \langle (V_1 - V_2)^2 \rangle = C_V^2 R^{2/3}, \quad l_0 \ll R \ll L_0, \tag{1}$$

where V_1, V_2 represent velocity components at two points separated by distance R and C_V^2, the velocity *structure constant* (in units of $\mathrm{m}^{4/3}/\mathrm{s}^2$), is a measure of the total amount of energy in the turbulence. The structure constant is related to the average energy dissipation rate ε by

$$C_V^2 = 2\varepsilon^{2/3}. \tag{2}$$

The velocity inner scale l_0 [m], which forms the lower limit of the inertial range characterized by the $2/3$ power law relation (1), is on the order of the *Kolmogorov microscale* η, i.e., [5]

$$l_0 \sim \eta = (\nu^3/\varepsilon)^{1/4}. \tag{3}$$

The inverse dependence of inner scale on the average rate of dissipation ε as given in Eq. (3) shows that strong turbulence has smaller inner scales and weak turbulence has larger inner scales. The outer scale L_0, which defines the upper limit in the structure function relation (1), is proportional to $\varepsilon^{1/2}$. Thus, unlike the inner scale, the outer scale L_0 increases and decreases directly with the strength of turbulence.

The behavior of the longitudinal structure function at small-scale sizes ($R \ll l_0$) varies with the square of separation distance R. This quadratic behavior is easily inferred from a Taylor series expansion of the structure function at small distances [see Eq. (59) in Chap. 2]. The constant of proportionality is chosen so that the two power laws agree when $R = l_0$, which, when combined with (1), leads to the asymptotic forms [6]

$$D_{RR}(R) = \begin{cases} C_V^2 l_0^{-4/3} R^2, & 0 \le R \ll l_0 \\ C_V^2 R^{2/3}, & l_0 \ll R \ll L_0. \end{cases} \tag{4}$$

The R^2 and $R^{2/3}$ power-law behavior of the above velocity structure function (scaled by $C_V^2 l_0^{2/3}$) is shown in Fig. 3.2 (dashed curves) for separation distance scaled by the inner scale. It is the intersection of these two asymptotic curves that in fact defines the inner scale l_0 (i.e., the point of intersection at which $R = l_0$). The solid curve depicts the continuous behavior of the scaled structure function in terms of R/l_0 as it transitions between the two asymptotic expressions given in (4).

Because the random field of velocity fluctuations is basically nonisotropic for scale sizes larger than the outer scale L_0, no general description of the structure

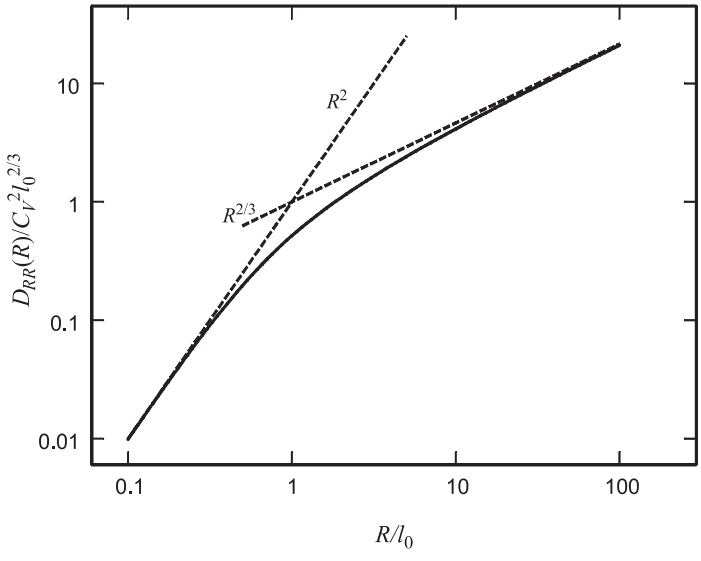

Figure 3.2 The scaled longitudinal velocity structure function showing both R^2 and $R^{2/3}$ asymptotic domains (dashed lines).

function can be predicted for $R > L_0$. However, if the random velocity field was strictly homogeneous and isotropic, even for large separation distances, the structure function would asymptotically approach the value $2\sigma_V^2$, where σ_V^2 is the variance of the longitudinal velocity fluctuations.

The $2/3$ power law behavior of the structure function in the inertial range is equivalent to the power spectrum in three dimensions given by

$$\begin{aligned}\Phi_{RR}(\kappa) &= 0.066\varepsilon^{2/3}\kappa^{-11/3} \\ &= 0.033C_V^2\kappa^{-11/3}, \quad 1/L_0 \ll \kappa \ll 1/l_0,\end{aligned} \tag{5}$$

where κ is the scalar spatial frequency (in units of rad/m). Observe that the power spectrum (5) exhibits a $-11/3$ power law, which corresponds to a one-dimensional spectrum with a $-5/3$ power law (Section 2.6). The validity of the $2/3$ power law for the structure function and $-11/3$ power law associated with the power spectrum have been established over a wide range of experiments [7]. However, a number of papers [8–11] devoted to the intermittent nature of turbulence resulting in random spatial fluctuations of the local dissipation rate suggest a modest change in the power law behavior of the structure function from $2/3$ to approximately $2/3 + 0.025$. Such small changes have little effect on second-order statistical quantities of interest in our work, like structure functions or power spectral densities, but may be important in higher-order statistics.

3.2.2 Temperature fluctuations

Historically, the fundamental ideas and characterization of turbulence were developed in terms of the velocity fluctuations. However, the basic ideas of Kolmogorov concerning velocity fluctuations have also been applied to conservative passive scalars such as potential temperature[1] (rather than absolute temperature) [8]. Temperature fluctuations are considered passive because they do not exchange energy with the velocity turbulence. An associated inner scale l_0 and outer scale L_0 of the small-scale temperature fluctuations form the lower and upper boundaries of the inertial range or, in the case of temperature fluctuations, the *inertial-convective range.* Also, the dissipation mechanism for temperature inhomogeneities is molecular diffusion, not viscosity as in the case of velocity fluctuations. By extending the Kolmogorov theory of structure functions given above to statistically homogeneous and isotropic temperature fluctuations, we are led to the same power law relations as found with longitudinal velocity fluctuations, viz.,

$$D_T(R) = \langle (T_1 - T_2)^2 \rangle = \begin{cases} C_T^2 l_0^{-4/3} R^2, & 0 \le R \ll l_0 \\ C_T^2 R^{2/3}, & l_0 \ll R \ll L_0, \end{cases} \tag{6}$$

[1]The potential temperature θ is related to absolute temperature T by $\theta = T + \alpha_a h$, where α_a is called the adiabatic rate of decrease of the temperature and h is height above the Earth's surface. For a small range of height, we can neglect the adiabatic rate α_a and treat T as a passive scalar as we do here.

where T_1, T_2 denote the temperature at two points separated by distance R and C_T^2 is the temperature *structure constant* (in units of $\mathrm{deg}^2/\mathrm{m}^{2/3}$). The inner scale for temperature, which is of the same order of magnitude as the inner scale for velocity fluctuations, is given by [12]

$$l_0 = 5.8(D^3/\varepsilon)^{1/4}, \tag{7}$$

where D is the diffusivity of heat in air (in units of m^2/s).

Based on the $2/3$ power law behavior of the structure function (6) in the inertial-convective range, the three-dimensional spectrum of temperature fluctuations takes the $-11/3$ power-law form

$$\begin{aligned}\Phi_T(\kappa) &= \frac{1}{4\pi}\beta\chi\varepsilon^{-1/3}\kappa^{-11/3} \\ &= 0.033C_T^2\kappa^{-11/3}, \quad 1/L_0 \ll \kappa \ll 1/l_0,\end{aligned} \tag{8}$$

where β is the Obukhov-Corrsin constant and χ is the rate of dissipation of mean-squared temperature fluctuations. Although not contained in Eq. (8), Hill and Clifford [12] have pointed out that the temperature spectrum at high wave numbers actually contains a small "bump" near $1/l_0$ that can have important consequences on a number of statistical quantities important in problems involving optical wave propagation. That is, the bump in the temperature spectrum also induces a corresponding spectral bump in the spectrum of refractive-index fluctuations as discussed below in Section 3.3.

3.2.3 Refractive-index fluctuations

The index of refraction n, one of the most significant parameters of the atmosphere for optical wave propagation, is very sensitive to small-scale temperature fluctuations. In particular, temperature fluctuations combined with turbulent mixing induce a random behavior in the field of atmospheric index of refraction. At a point $\mathbf{R}$ in space and time t, the index of refraction can be mathematically expressed by

$$n(\mathbf{R}, t) = n_0 + n_1(\mathbf{R}, t), \tag{9}$$

where $n_0 = \langle n(\mathbf{R}, t)\rangle \cong 1$ is the mean value of the index of refraction and $n_1(\mathbf{R}, t)$ represents the random deviation of $n(\mathbf{R}, t)$ from its mean value; thus, $\langle n_1(\mathbf{R}, t)\rangle = 0$. Time variations in the refractive index are often suppressed in the treatment of optical wave propagation. This means that the wave maintains a single frequency as it propagates. It is customary, therefore, to express Eq. (9) in the form

$$n(\mathbf{R}) = 1 + n_1(\mathbf{R}), \tag{10}$$

where $n(\mathbf{R})$ has been normalized by its mean value n_0.

Fluctuations in the index of refraction are related to corresponding temperature and pressure fluctuations. In particular, the index of refraction for the atmosphere

can be written for optical and IR wavelengths according to [13]

$$n(\mathbf{R}) = 1 + 77.6 \times 10^{-6}(1 + 7.52 \times 10^{-3}\lambda^{-2})\frac{P(\mathbf{R})}{T(\mathbf{R})}$$

$$\cong 1 + 79 \times 10^{-6}\frac{P(\mathbf{R})}{T(\mathbf{R})}, \tag{11}$$

where λ is the optical wavelength in μm, P is the pressure in millibars, and T is the temperature in kelvin. The wavelength dependence is small for optical frequencies, so we have set $\lambda \sim 0.5$ μm as typical in the second expression in (11). Because pressure fluctuations are usually negligible, we see that index-of-refraction fluctuations associated with the visible and near-IR region of the spectrum are due primarily to random temperature fluctuations (humidity fluctuations only contribute in the far-IR region). Changes in the optical signal due to absorption or scattering by molecules or aerosols are not considered here.

The statistical description of the random field of turbulence-induced fluctuations in the atmospheric refractive index is similar to that for the related random field of turbulent velocities. In particular, an inertial subrange exists bounded above by an *outer scale* L_0 and below by an *inner scale* l_0. Also, when exhibited by the field of velocity fluctuations within the inertial subrange, the properties of statistical homogeneity and isotropy are inherited by the field of refractive-index fluctuations within the corresponding inertial subrange.

Because $\langle n_1(\mathbf{R})\rangle = 0$, the *covariance function* of $n(\mathbf{R})$ can be expressed as

$$B_n(\mathbf{R}_1, \mathbf{R}_2) \equiv B_n(\mathbf{R}_1, \mathbf{R}_1 + \mathbf{R}) = \langle n_1(\mathbf{R}_1)n_1(\mathbf{R}_1 + \mathbf{R})\rangle,$$

which, if the random field of refractive-index fluctuations is *statistically homogeneous*, is a function of $\mathbf{R} = \mathbf{R}_1 - \mathbf{R}_2$. If the random field is both *statistically homogeneous* and *isotropic*, the covariance function further reduces to a function of only the scalar distance $R = |\mathbf{R}_1 - \mathbf{R}_2|$.[2] For statistically homogeneous and isotropic turbulence, the related *structure function* exhibits the asymptotic behavior

$$D_n(R) = 2[B_n(0) - B_n(R)] = \begin{cases} C_n^2 l_0^{-4/3} R^2, & 0 \le R \ll l_0 \\ C_n^2 R^{2/3}, & l_0 \ll R \ll L_0, \end{cases} \tag{12}$$

where C_n^2 is the index-of-refraction *structure constant* (in units of $\mathrm{m}^{-2/3}$), sometimes called the *structure parameter*, and the inner scale is [6,12]

$$l_0 = 7.4\eta = 7.4(\nu^3/\varepsilon)^{1/4}. \tag{13}$$

Physically, the refractive-index structure constant C_n^2 is a measure of the strength of the fluctuations in the refractive index. Behavior of C_n^2 at a point along the propagation path can be deduced from the temperature structure function obtained from *point measurements* of the mean-square temperature difference of

[2]In Chap. 5 we will introduce the *Markov approximation*, which assumes the covariance function is delta correlated in the direction of propagation (positive z-axis). Even in this case, we can assume it remains statistically homogeneous and isotropic in the transverse direction.

two fine wire thermometers. In this case, the temperature structure constant C_T^2 is calculated by use of Eq. (6) and values of C_n^2 can be inferred directly from Eq. (11), which leads to

$$C_n^2 = \left(79 \times 10^{-6} \frac{P}{T^2}\right)^2 C_T^2. \tag{14}$$

Path-averaged values of C_n^2 and inner scale l_0 can be obtained simultaneously by optical measurements over a short path length (typically 150 m) using an instrument called a scintillometer [14]. Figures 3.3 and 3.4 illustrate standard behavior of C_n^2 and l_0 as measured 1.5 m above the ground by a scintillometer over 6 daytime hours of a typical winter day in Central Florida (with partially cloudy skys and low wind speeds). However, the data in these figures are qualitatively representative of general near-ground behavior of these atmospheric parameters at other geographical locations. If measured over a 24-hour period, the C_n^2 data would clearly show a diurnal cycle with a well-defined peak during mid-day hours, near constant values at night, and minima near sunrise and sunset.

Values of C_n^2 typically range from 10^{-17} $\mathrm{m}^{-2/3}$ or less for conditions of "weak turbulence" and up to 10^{-13} $\mathrm{m}^{-2/3}$ or more when the turbulence is "strong." Over short time intervals at a fixed propagation distance and constant height above the ground it may be reasonable to assume that C_n^2 is essentially constant. However, for vertical and slant propagation paths the refractive-index structure parameter varies as a function of height above ground (Section 12.2).

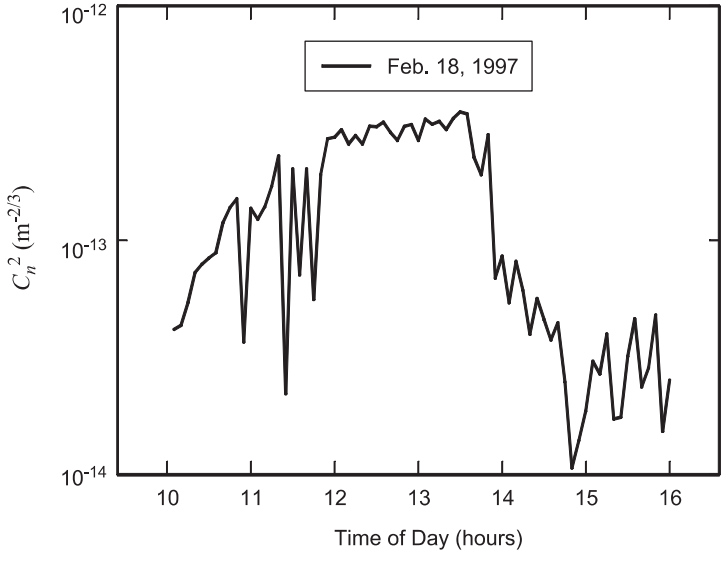

Figure 3.3 Path-averaged values of the refractive-index structure parameter 1.5 m above ground level.

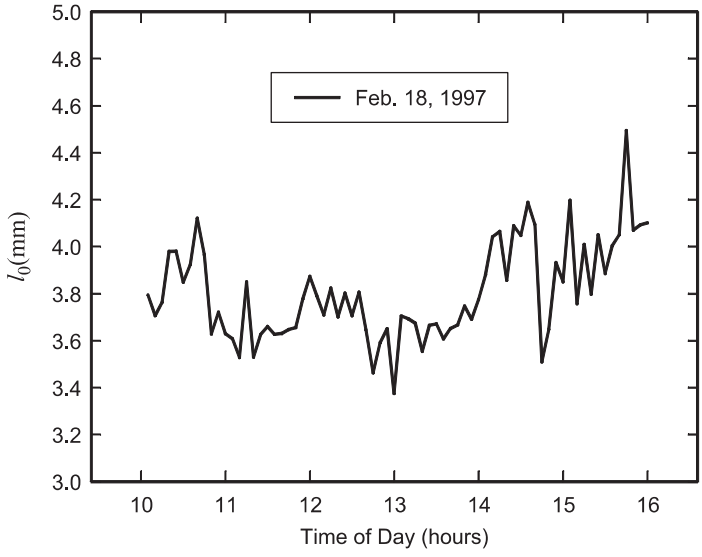

Figure 3.4 Path-averaged values of the inner scale 1.5 m above ground level.

3.3 Power Spectrum Models for Refractive-Index Fluctuations

Under the assumption of a statistically homogeneous and isotropic atmosphere, the *spatial power spectral density* of refractive-index fluctuations is related to the covariance function by the three-dimensional Fourier transform

$$\begin{aligned}\Phi_n(\kappa) &= \frac{1}{(2\pi)^3}\int\int\int_{-\infty}^{\infty} B_n(R)\exp(-i\mathbf{K}\cdot\mathbf{R})\,d^3R \\ &= \frac{1}{2\pi^2\kappa}\int_0^{\infty} B_n(R)\sin(\kappa R)R\,dR,\end{aligned} \tag{15}$$

where spherical symmetry has been used to obtain the last integral and $\kappa = |\mathbf{K}|$ is the scalar wave number. By properties of the inverse Fourier transform it also follows that

$$B_n(R) = \frac{4\pi}{R}\int_0^{\infty} \kappa\Phi_n(\kappa)\sin(\kappa R)\,d\kappa, \tag{16}$$

and, consequently, the relation between the spectrum and structure function can be expressed by

$$\begin{aligned}D_n(R) &= 2[B_n(0) - B_n(R)] \\ &= 8\pi\int_0^{\infty} \kappa^2\Phi_n(\kappa)\left(1 - \frac{\sin\kappa R}{\kappa R}\right)d\kappa.\end{aligned} \tag{17}$$

3.3.1 Kolmogorov spectrum

For optical wave propagation, refractive-index fluctuations are caused almost exclusively by small fluctuations in temperature. That is, variations in humidity and pressure can usually be neglected. It is generally accepted, therefore, that the functional form of the spatial power spectrum of refractive-index fluctuations is the same as that for temperature and, further, that temperature fluctuations obey the same spectral laws as velocity fluctuations. Based on the inertial subrange $2/3$ power law expression in Eq. (12) for the structure function, it can be deduced that the associated power spectral density for refractive-index fluctuations over the inertial subrange is defined by

$$\Phi_n(\kappa) = 0.033 C_n^2 \kappa^{-11/3}, \quad 1/L_0 \ll \kappa \ll 1/l_0. \tag{18}$$

Equation (18) is the well-known *Kolmogorov power-law spectrum.* Partly because of its relatively simple mathematical form, it is widely used in theoretical calculations. Nonetheless, this spectrum model is theoretically valid only over the inertial subrange $1/L_0 \ll \kappa \ll 1/l_0$ as stated in (18). To justify its use in certain calculations over all wave numbers, it is ordinarily assumed that the outer scale is infinite ($L_0 = \infty$) and the inner scale is negligibly small ($l_0 = 0$). However, extending the validity of (18) to all wave numbers may lead to divergent integrals in some cases. Some care must therefore be exercised in the use of this spectrum model.

3.3.2 Tatarskii, von Kármán, and exponential spectrums

Other spectrum models have been proposed for making calculations when inner scale and/or outer scale effects cannot be ignored. The extension of the power law spectrum (18) into the dissipation range $\kappa > 1/l_0$ requires the introduction of a function that essentially truncates the spectrum at high wave numbers. For purposes of mathematical convenience, Tatarskii [6] suggested doing this with a Gaussian function, which led to the spectrum model[3]

$$\Phi_n(\kappa) = 0.033 C_n^2 \kappa^{-11/3} \exp\left(-\frac{\kappa^2}{\kappa_m^2}\right), \qquad \kappa \gg 1/L_0; \qquad \kappa_m = 5.92/l_0. \tag{19}$$

Actually, Eq. (19), which is widely called the *Tatarskii spectrum*, was first proposed by Novikov [15] for velocity fluctuations and later adopted by Tatarskii for refractive-index fluctuations.

Like the Kolmogorov spectrum (18), the Tatarskii spectrum (19) has a singularity at $\kappa = 0$ for the limiting case $1/L_0 = 0$ ($L_0 \to \infty$). This means, for example, that the structure function $D_n(R)$ [Eq. (17)] can be calculated but the covariance function $B_n(R)$ [Eq. (16)] cannot. Although atmospheric turbulence is almost always locally homogeneous and isotropic, the spatial power spectrum is isotropic

[3]The proportionality constant 5.92 in Eq. (19) is chosen to produce the quadratic power-law form of the structure function in Eq. (13). See, for instance, Example 1 in the Worked Examples.

only in the inertial subrange or dissipation range for which $\kappa > 1/L_0$. For the input range $\kappa < 1/L_0$, the spectrum is generally considered anisotropic and its form is not known.

The Kolmogorov and Tatarskii spectrum models are often modified in practice so that they are also finite and isotropic for wave numbers $\kappa < 1/L_0$. When this is done the corresponding structure function and covariance function both exist. In the case of a modification of the Tatarskii spectrum, the turbulence is modeled as if it were statistically homogeneous and isotropic over *all* wave numbers. Spectral models that are often used in this regard are

$$\Phi_n(\kappa) = \begin{cases} \dfrac{0.033C_n^2}{(\kappa^2 + \kappa_0^2)^{11/6}}, & 0 \le \kappa \ll 1/l_0 \\ 0.033C_n^2 \dfrac{\exp(-\kappa^2/\kappa_m^2)}{(\kappa^2 + \kappa_0^2)^{11/6}}, & 0 \le \kappa < \infty; \qquad \kappa_m = 5.92/l_0, \end{cases} \tag{20}$$

where $\kappa_0 = 2\pi/L_0$ (or sometimes $\kappa_0 = 1/L_0$). The upper expression in (20), which only includes the outer scale parameter κ_0, is the original form of this model called the *von Kármán spectrum.* The Gaussian function inner scale term in the numerator of the lower expression was introduced later by others to combine the Tatarskii and von Kármán spectrums into one that included both inner scale and outer scale effects. Consequently, it is called the *modified von Kármán spectrum.* However, both forms are often referred to as simply the von Kármán spectrum. In the inertial subrange $\kappa_0 \ll \kappa \ll \kappa_m$, Eqs. (19) and (20) both reduce to the Kolmogorov power-law spectrum defined above by Eq. (18).

Another spectrum model with outer scale parameter is the *exponential spectrum*

$$\Phi_n(\kappa) = 0.033C_n^2\kappa^{-11/3}[1 - \exp(-\kappa^2/\kappa_0^2)], \quad 0 \le \kappa \ll 1/l_0. \tag{21}$$

Here the outer scale parameter κ_0 is related to outer scale in general by $\kappa_0 = C_0/L_0$, where the scaling constant C_0 is chosen differently depending on the application. For example, to approximate the von Kármán spectrum we might set $C_0 = 4\pi$ (see Example 2 in the Worked Examples), whereas in our scintillation model introduced in Chap. 9, we use $C_0 = 8\pi$. Because the outer scale itself is not well defined, it is difficult to proclaim any particular constant C_0 with the outer scale parameter κ_0.

3.3.3 Modified atmospheric spectrum

Spectrum models (19) through (21) are relatively tractable models. For that reason, they are commonly used in theoretical studies of optical wave propagation. Strictly speaking, however, these spectrum models have the correct behavior only in the inertial range. That is, the mathematical form that permits the use of these spectrums outside the inertial range is based on mathematical convenience, not physical models. None of these spectrums, for instance, features the small rise (or bump) at high wave numbers near $1/l_0$ that causes the spectrum to decrease less rapidly than predicted by the $\kappa^{-11/3}$ law of Obukhov [16] and Corrsin [17].

This so-called bump is clearly revealed in the temperature data of Champagne et al. [18] and in that of Williams and Paulson [19]. Because the refractive index obeys the same spectral law as temperature, the bump must also appear in the spectrum of refractive-index fluctuations. Hill [20] performed a hydrodynamic analysis that led to a numerical spectral model with a high wave number rise that accurately fit the experimental data in Refs. [18] and [19]. The impact of the Hill numerical spectrum on optical wave propagation was soon pointed out by Hill and Clifford [12]. In general, it was concluded that the presence of a bump in the refractive-index spectrum produces a corresponding bump in many measurable quantities like structure functions and scintillation index. A theoretical foundation for the bump spectrum can also be found in Dubovikov and Tatarskii [21] and in Tatarskii et al. [22].

Andrews [23] developed an analytic approximation to the Hill spectrum, including an outer scale parameter, that offers the same tractability for theoretical purposes as the von Kármán spectrum (20). This approximation, which we henceforth refer to as the *modified atmospheric spectrum* (or, simply, the *modified spectrum*), is given by

$$\Phi_n(\kappa) = 0.033C_n^2\left[1 + 1.802\left(\frac{\kappa}{\kappa_l}\right) - 0.254\left(\frac{\kappa}{\kappa_l}\right)^{7/6}\right]\frac{\exp(-\kappa^2/\kappa_l^2)}{(\kappa^2+\kappa_0^2)^{11/6}}, \qquad (22)$$

$$0 \le \kappa < \infty; \qquad \kappa_l = 3.3/l_0,$$

where, similar to the von Kármán spectrum, $\kappa_0 = 2\pi/L_0$ (or $\kappa_0 = 1/L_0$). Once again, the choice of scaling constant is not clear. Note that (22) is similar to the functional form of (20), except for the terms within the brackets [ ] that characterize the high wave number spectral bump. Rather than introduce the outer scale parameter in the manner adopted from the von Kármán spectrum, we can choose to write the modified spectrum in the form

$$\Phi_n(\kappa)=0.033C_n^2\left[1+1.802\left(\frac{\kappa}{\kappa_l}\right)-0.254\left(\frac{\kappa}{\kappa_l}\right)^{7/6}\right]\left[1-\exp\left(-\frac{\kappa^2}{\kappa_0^2}\right)\right]\frac{\exp(-\kappa^2/\kappa_l^2)}{\kappa^{11/3}},$$

$$0\le\kappa<\infty; \qquad \kappa_l=3.3/l_0, \qquad \kappa_0=4\pi/L_0, \qquad (23)$$

where, in some cases, we might instead define $\kappa_0=2\pi/L_0$ or $\kappa_0=8\pi/L_0$.

In Fig. 3.5 the Kolmogorov spectrum (18), von Kármán spectrum (20), and modified atmospheric spectrum (22) are illustrated over a range of wave numbers, showing the outer scale and inner scale wave numbers that identify the boundaries of the inertial subrange. Also shown in Fig. 3.5 is the high wave number bump just prior to the dissipation range (which is greatly suppressed by the logarithmic scale). A nonzero inner scale reduces values of the spectrum at high wave numbers ($\kappa > l_0$) over that predicted by the Kolmogorov spectrum. At low wave numbers ($\kappa < 1/L_0$), a similar reduction in values of the spectrum are caused by the presence of a finite outer scale. The Hill numerical spectrum, along with spectral models (19) and (22) (with $\kappa_0 = 0$), all scaled by the Kolmogorov power law spectrum, are shown in Fig. 3.6 where the characteristic

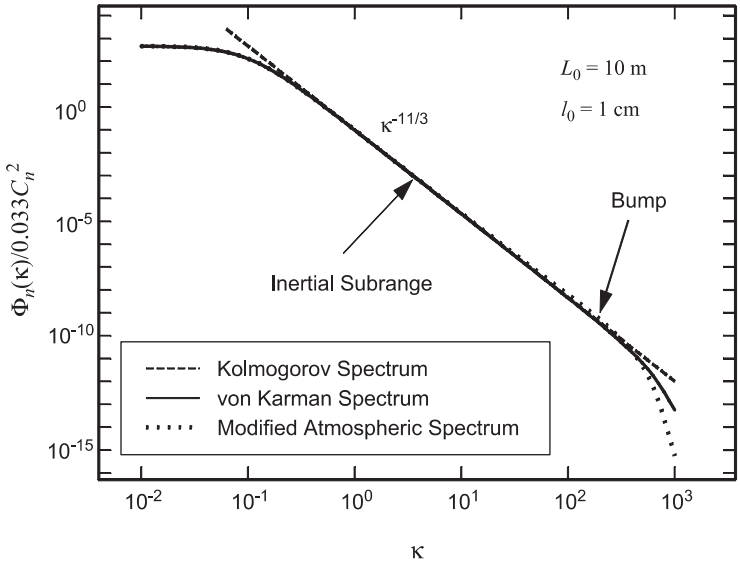

Figure 3.5 Spectral models of refractive-index fluctuations.

bump in the spectrum is more clearly revealed. Other analytic approximations to the Hill spectrum have been developed by Churnside [24] and by Frehlich [25].

The general effect of the modified spectrum on various statistical quantities can be observed by considering the refractive-index structure function. That is, the analytic form of the refractive-index structure function based on the Tatarskii

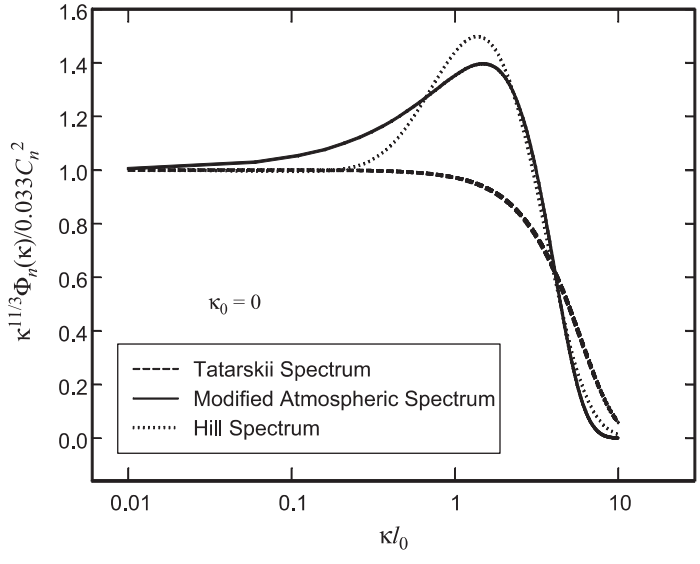

Figure 3.6 Scaled spectral models of refractive-index fluctuations plotted as a function of κl_0.

spectrum (19) is given by (see Prob. 2)

$$D_n(R) = 1.685 C_n^2 \kappa_m^{-2/3} \left[{}_1F_1\left(-\frac{1}{3};\ \frac{3}{2};\ -\frac{\kappa_m^2 R^2}{4} \right) - 1 \right], \quad 0 \le R \ll L_0, \tag{24}$$

where ${}_1F_1(a, c, x)$ is a confluent hypergeometric function [26] (also, see Appendix I). On the other hand, that based on the modified spectrum (22), with $\kappa_0 = 0$, is (see Prob. 6)

$$\begin{aligned} D_n(R) = 1.685 C_n^2 \kappa_l^{-2/3} \Bigg\{ & {}_1F_1\left(-\frac{1}{3};\ \frac{3}{2};\ -\frac{\kappa_l^2 R^2}{4} \right) - 1 \\ & + 2.470 \left[1 - {}_1F_1\left(\frac{1}{6};\ \frac{3}{2};\ -\frac{\kappa_l^2 R^2}{4} \right) \right] \\ & - 0.071 \left[1 - {}_1F_1\left(\frac{1}{4};\ \frac{3}{2};\ -\frac{\kappa_l^2 R^2}{4} \right) \right] \Bigg\}, \quad 0 \le R \ll L_0. \end{aligned} \tag{25}$$

In Fig. 3.7 the scaled structure function $D_n(R)/C_n^2 l_0^{2/3}$ is plotted as a function of R/l_0. The solid curve corresponds to Eq. (25) using the modified spectrum and the dashed curve represents Eq. (24) derived from the Tatarskii spectrum. Here, we see that the bump in the modified spectrum at high wave numbers produces a corresponding bump in the structure function at separation distance $R \sim 2l_0$. When calculating other statistical quantities with the modified spectrum, similar disparities are found in comparison with results based on more conventional spectrum models.

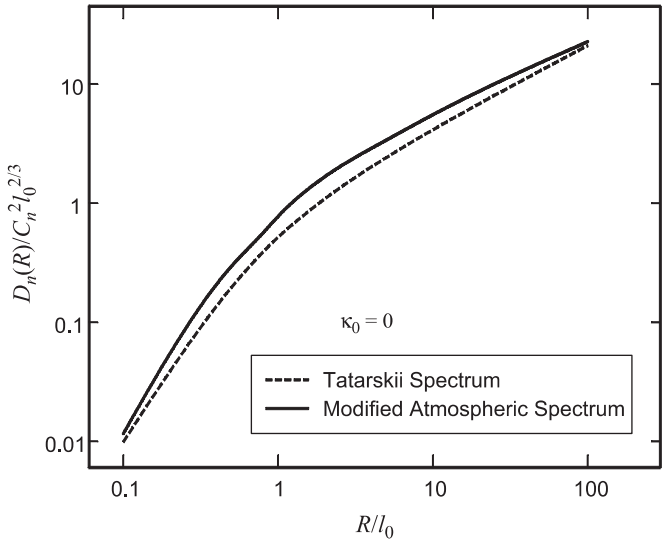

Figure 3.7 Scaled structure function of refractive index plotted as a function of separation distance R scaled by the inner scale l_0. The outer scale is assumed infinite (i.e., $\kappa_0 = 0$).

3.3.4 Variation of C_n^2 with propagation distance

In some situations of practical interest we find that the strength of turbulence as predicted by the refractive-index structure parameter C_n^2 will vary as a function of propagation distance. For example, in slant paths and vertical paths through the atmosphere, such as those associated with satellite communication channels (see Chap. 12) or astronomy applications, the value of structure parameter C_n^2 will vary as a function of altitude, location, and time of day. We use the notation $C_n^2(z)$ to denote the dependence of turbulence strength on propagation path length and $\Phi_n(\kappa, z)$ to represent the corresponding spatial power spectrum. For example, the Kolmogorov spectrum (18) under these conditions takes the form

$$\Phi_n(\kappa, z) = 0.033 C_n^2(z) \kappa^{-11/3}. \tag{26}$$

In some cases, it may be necessary to include variations of inner scale and outer scale parameters as a function of path length z when using other spectrum models.

Extensive experimental measurements of C_n^2 as a function of altitude above the Earth's surface have been made over the years [27–41]. Data from these measurements have led to several mathematical models of C_n^2, but these models are largely dependent upon geographical location and other local conditions. Some of these models are reviewed in Section 12.2.1, but a more comprehensive treatment can be found in Beland [39].

3.4 Atmospheric Temporal Statistics

The statistical averages of the random field discussed in this chapter are called ensemble averages, whereas in Chap. 2 we were also concerned with temporal averages. To draw a connection between the two types of statistical averaging in our physical model of the atmosphere, we make use of the so-called "frozen turbulence" hypothesis of Taylor. This hypothesis says that temporal variations of meteorological quantities at a point are produced by advection of these quantities by the mean wind speed flow and not by changes in the quantities themselves. This is similar to the idea of clouds moving at a particular speed with little change in shape over small time intervals. Thus, with knowledge of the mean wind speed, we can directly convert from spatial statistics to temporal statistics.

To elaborate on the above discussion, we note that in the atmosphere there are essentially two time scales of concern—one that is due to motion of the atmosphere across the path of observation and the other resulting from dynamics of the turbulence (i.e., eddies). The first time scale, that due to advection, can be estimated by $L_0/V_\perp$, where L_0 is the outer scale of turbulence and $V_\perp$ is the mean wind speed transverse to the observation path. This time scale is typically on the order of 1 s. The second time scale, associated with the eddy turnover

time, is much slower, typically on the order of 10 s. Because the second time scale is much slower than the first, it can ordinarily be neglected in comparison with the mean wind flow. Hence, under the *Taylor frozen turbulence hypothesis*, turbulent eddies are treated as frozen in space and moved across the observation path by the mean wind speed component $V_\perp$. A turbulence variable $u(\mathbf{R}, t)$ in this case has time dependence given by the expression

$$u(\mathbf{R}, t + \tau) = u(\mathbf{R} - \mathbf{V}_\perp \tau, t) \tag{27}$$

for any time t. Experimental evidence seems to support the reasonableness of this expression. However, Taylor's hypothesis fails when $V_\perp$ is considerably less than the magnitude of turbulent fluctuations in wind velocity, such as occurs when the mean wind speed is parallel (or near parallel) to the line of sight.

3.5 Summary and Discussion

When the flow of a viscous fluid exceeds a critical *Reynolds number*, the flow changes from laminar to a more chaotic state called *turbulence*. Turbulent air motion represents a set of vortices, or eddies, of various scale sizes, extending from a large scale size L_0 called the *outer scale* of turbulence to a small scale size l_0 called the *inner scale* of turbulence. Under the influence of inertial forces, large eddies break up into smaller ones, forming a continuous cascade of scale sizes between L_0 and l_0 known as the *inertial range*. Scale sizes smaller than the inner scale belong to the *dissipation range*.

In the atmosphere, turbulent fluctuations in wind speed result in the mixing of atmospheric quantities such as temperature, water vapor, and the index of refraction. These quantities are called *passive scalars* because their dynamics do not affect the turbulence associated with velocity fluctuations. The most important of these quantities in optical wave propagation is the *index-of-refraction fluctuations*, commonly referred to as *optical turbulence*. Because it behaves like a passive additive, the theoretical framework of optical turbulence is based on the classical theory of turbulence concerning velocity fluctuations.

Of particular significance is the fact that the *structure function* of the index of refraction obeys a $2/3$ power law in the inertial range, the same as obtained for temperature and longitudinal velocity fluctuations [e.g., see Eqs. (1) and (6)]. The corresponding inertial range behavior of the *three-dimensional power spectrum* of index-of-refraction fluctuations is, therefore, described by a $-11/3$ power law, viz., the *Kolmogorov spectrum*

$$\Phi_n(\kappa) = 0.033 C_n^2 \kappa^{-11/3}, \quad 1/L_0 \ll \kappa \ll 1/l_0. \tag{28}$$

The Kolmogorov spectrum is undoubtedly the most commonly used spectrum in theoretical analyses but it is appropriate only over wave numbers within the inertial range. To account for the behavior of the power spectrum outside the inertial

range, various spectral models have been proposed. These models include the *Tatarskii spectrum*:

$$\Phi_n(\kappa) = 0.033 C_n^2 \kappa^{-11/3} \exp\left(-\frac{\kappa^2}{\kappa_m^2}\right), \quad \kappa \gg 1/L_0; \qquad \kappa_m = 5.92/l_0, \tag{29}$$

the (modified) *von Kármán spectrum*:

$$\Phi_n(\kappa) = 0.033 C_n^2 \frac{\exp(-\kappa^2/\kappa_m^2)}{(\kappa^2 + \kappa_0^2)^{11/6}}, \quad 0 \le \kappa < \infty; \qquad \kappa_m = 5.92/l_0, \tag{30}$$

and the *modified amospheric spectrum*:

$$\begin{aligned} \Phi_n(\kappa) = 0.033 C_n^2 &\left[1 + 1.802(\kappa/\kappa_l) - 0.254(\kappa/\kappa_l)^{7/6}\right] \\ &\times \frac{\exp(-\kappa^2/\kappa_l^2)}{(\kappa^2 + \kappa_0^2)^{11/6}}, \quad 0 \le \kappa < \infty; \qquad \kappa_l = 3.3/l_0. \end{aligned} \tag{31}$$

These latter models (29)–(31) are not based on rigorous calculations outside the inertial range, but more on mathematical convenience and tractability. Only the modified atmospheric spectrum (31) features the high wave number rise prior to the dissipation range that is of particular importance in scintillation studies.

3.6 Worked Examples

Example 1: Given the Tatarskii spectrum model (19) and the structure function

$$D_n(R) = 8\pi \int_0^\infty \kappa^2 \Phi_n(\kappa) \left(1 - \frac{\sin \kappa R}{\kappa R}\right) d\kappa,$$

derive Eq. (24) and use asymptotic relations to deduce those in Eq. (12). In doing so, establish that the scaling constant for the parameter $\kappa_m = \alpha/l_0$ is $\alpha = 5.92$.

Solution: To begin, we will discuss a technique for determining the structure function given by (22). Although it is tempting to split the defining integral into two integrals

$$D_n(R) = 8\pi \int_0^\infty \kappa^2 \Phi_n(\kappa)\, d\kappa - \frac{8\pi}{R} \int_0^\infty \kappa \Phi_n(\kappa) \sin \kappa R\, d\kappa,$$

neither of these integrals converges with spectral model (19) because of the singularity at $\kappa = 0$. Instead, we can expand the term $1 - (\sin \kappa R)/\kappa R$ of the original single integral in a Maclaurin series and termwise integrate the resulting sum

of convergent integrals (see Prob. 2). By summing the series after termwise integration, this action leads to

$$D_n(R) = 1.685 C_n^2 \kappa_m^{-2/3} \left[{}_1F_1\left(-\frac{1}{3}; \frac{3}{2}; -\frac{\kappa_m^2 R^2}{4} \right) - 1 \right], \quad 0 \le R \ll L_0.$$

Properties of the confluent hypergeometric function ${}_1F_1(a; c; -x)$ are given in Ref. [26] and reviewed in Appendix I for easy reference. In particular, at sufficiently large separation distances ($l_0 \ll R \ll L_0$), we can use the large argument asymptotic formula

$${}_1F_1(a; c; -x) \sim \frac{\Gamma(c)}{\Gamma(c-a)} x^{-a}, \quad x \gg 1,$$

where $\Gamma(x)$ is the gamma function, to deduce the $2/3$ power-law relation

$$D_n(R) = C_n^2 R^{2/3}, \quad l_0 \ll R \ll L_0.$$

On the other hand, for $R \ll l_0$, we use the small argument relation

$${}_1F_1(a; c; -x) \sim 1 - \frac{a}{c} x, \quad x \ll 1,$$

which leads to

$$D_n(R) = 0.0936 C_n^2 \kappa_m^{4/3} R^2, \quad R \ll l_0.$$

By assuming $\kappa_m = \alpha / l_0$, we see that $\alpha = 5.92$ (or, perhaps, 5.91) in order that this last expression agree with that in Eq. (12). ❑

Example 2: Graphically compare the von Kármán and exponential spectrums by plotting the scaled spectrum models

$$\textit{von Kármán}: \quad \frac{\kappa^{11/3} \Phi_n(\kappa)}{0.033 C_n^2} = \frac{\kappa^{11/3}}{\left(\kappa^2 + \kappa_0^2\right)^{11/6}},$$

$$\textit{Exponential}: \quad \frac{\kappa^{11/3} \Phi_n(\kappa)}{0.033 C_n^2} = 1 - \exp\left(-\frac{\kappa^2}{\kappa_0^2} \right).$$

Solution: For the von Kármán spectrum we set $\kappa_0 = 2\pi / L_0$, whereas for the exponential spectrum, we consider the cases $\kappa_0 = 2\pi / L_0$, $\kappa_0 = 4\pi \neq L_0$, and $\kappa_0 = 8\pi / L_0$. In Fig. 3.8 below, we show the graphs of these scaled spectrum models with outer scale parameter $L_0 = 1$ m. Here, we see that the two spectrum models are quite different if we use $\kappa_0 = 2\pi / L_0$ in both cases. However, by setting $\kappa_0 = 4\pi / L_0$ in the exponential spectrum we see that it more closely matches the von Kármán spectrum (with $\kappa_0 = 2\pi / L_0$). ❑

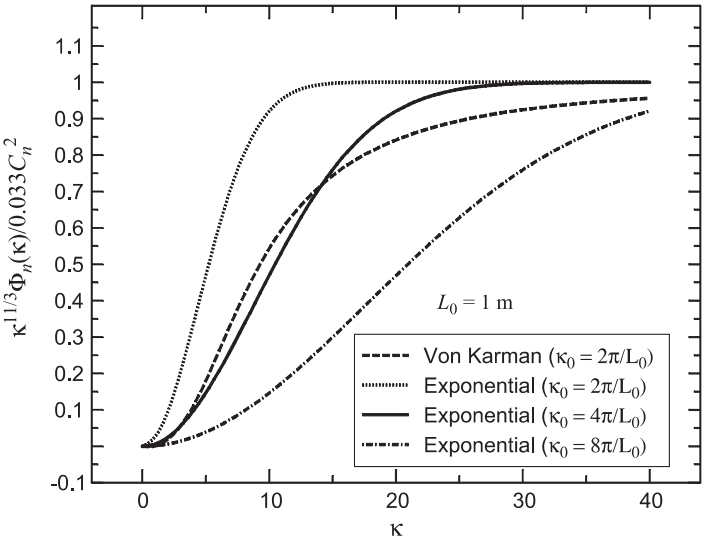

Figure 3.8 Scaled spectrums of the von Kármán and exponential models as a function of spatial wave number.

❑

Problems

Section 3.3

1. Given that the covariance $B_n(R)$ and the power spectral density $\Phi_n(\kappa)$ are related through the three-dimensional Fourier transform relation

$$\Phi_n(\kappa) = \frac{1}{(2\pi)^3} \int\int\int_{-\infty}^{\infty} B_n(R) \exp(-i\mathbf{K} \cdot \mathbf{R})\, d^3R,$$

   (*a*) show, by changing to spherical coordinates (R, θ, φ), that this transform relation simplifies to

$$\Phi_n(\kappa) = \frac{1}{2\pi^2 \kappa} \int_0^{\infty} B_n(R) \sin(\kappa R) R\, dR.$$

   Hint: Assume $\mathbf{K} \cdot \mathbf{R} = \kappa R \cos\varphi$.

   (*b*) Following along similar lines, deduce the inverse Fourier transform relation

$$B_n(R) = \frac{4\pi}{R} \int_0^{\infty} \kappa \Phi_n(\kappa) \sin(\kappa R)\, d\kappa.$$

2. By using the Maclaurin series representation

$$1 - \frac{\sin \kappa R}{\kappa R} = \sum_{n=1}^{\infty} \frac{(-1)^{n-1}}{(2n+1)!} \kappa^{2n} R^{2n},$$

   (*a*) show that the refractive index structure function (17), based on the Tatarskii spectrum (19), takes the form (assume termwise integration is permitted)

$$D_n(R) = 0.829 C_n^2 \sum_{n=1}^{\infty} \frac{(-1)^{n-1}}{(2n+1)!} R^{2n} \int_0^{\infty} \kappa^{2n-5/3} \exp(-\kappa^2/\kappa_m^2)\, d\kappa.$$

   (*b*) Use properties of the gamma function (see Appendix I) to deduce that

$$\int_0^{\infty} \kappa^{2n-5/3} \exp(-\kappa^2/\kappa_m^2)\, d\kappa = \frac{1}{2} \Gamma(n - 1/3) \kappa_m^{2n-2/3}.$$

   (*c*) Finally, use the result of (*b*) to show that the structure function in (*a*) can be expressed as

$$D_n(R) = 0.415 \Gamma(-1/3) C_n^2 \kappa_m^{-2/3} \left[1 - \sum_{n=0}^{\infty} \frac{(-1)^n (-1/3)_n}{(3/2)_n n!} \left(\frac{\kappa_m^2 R^2}{4} \right)^n \right]$$

$$= 1.685 C_n^2 \kappa_m^{-2/3} \left[{}_1F_1\left(-\frac{1}{3};\, \frac{3}{2};\, -\frac{\kappa_m^2 R^2}{4} \right) - 1 \right],$$

   where $(a)_n = \Gamma(a+n)/\Gamma(a)$ is the Pochhammer symbol (see Appendix I).

3. Retain only the first nonzero term of the series for $1 - (\sin \kappa R)/\kappa R$ in Prob. 2 to deduce

$$D_n(R) = C_n^2 l_0^{-4/3} R^2, \quad R \ll l_0.$$

4. Given that the power spectrum and structure function are related by

$$\Phi_n(\kappa) = \frac{1}{4\pi^2\kappa^2} \int_0^\infty \frac{\sin(\kappa R)}{\kappa R} \frac{\partial}{\partial R} \left[R^2 \frac{\partial D_n(R)}{\partial R} \right] dR,$$

use the structure function $D_n(R) = C_n^2 R^{2/3}$ and the integral formula

$$\int_0^\infty x^\alpha \sin x \, dx = 2^\alpha \sqrt{\pi} \frac{\Gamma(\alpha/2 + 1)}{\Gamma(1/2 - \alpha/2)}$$

to derive the Kolmogorov power-law spectrum (18).

5. Use the von Kármán spectrum (20) to deduce that the refractive-index structure function with inner scale and outer scale parameters can be approximated by[4]

$$D_n(R) = 1.685 C_n^2 \kappa_m^{-2/3} \left[{}_1F_1\left(-\frac{1}{3}; \frac{3}{2}; -\frac{\kappa_m^2 R^2}{4} \right) - 1 \right] + 1.05 C_n^2 \kappa_0^{-2/3} \left[1 - {}_0F_1\left(-; \frac{2}{3}; \frac{\kappa_0^2 R^2}{4} \right) \right], \quad \kappa_0 \ll \kappa_m.$$

6. Use the modified atmospheric spectrum (22) with $\kappa_0 = 0$ and the technique in Prob. 2 to deduce that the refractive-index structure function takes the form

$$D_n(R) = 1.685 C_n^2 \kappa_l^{-2/3} \left\{ {}_1F_1\left(-\frac{1}{3}; \frac{3}{2}; -\frac{\kappa_l^2 R^2}{4} \right) - 1 + 2.470 \left[1 - {}_1F_1\left(\frac{1}{6}; \frac{3}{2}; -\frac{\kappa_l^2 R^2}{4} \right) \right] - 0.071 \left[1 - {}_1F_1\left(\frac{1}{4}; \frac{3}{2}; -\frac{\kappa_l^2 R^2}{4} \right) \right] \right\}.$$

7. Given the von Kármán spectrum

$$\Phi_n(\kappa) = \frac{0.033 C_n^2}{\left(\kappa^2 + \kappa_0^2\right)^{11/6}},$$

(*a*) use the integral formula

$$\int_0^\infty \frac{x \sin(ax)}{(x^2 + b^2)^{p+1/2}} dx = \frac{\sqrt{\pi} b}{\Gamma(p + 1/2)} \left(\frac{a}{2b} \right)^n K_{1-p}(ab), \quad a > 0$$

[4]The absence of a numerator parameter in ${}_0F_1$ is emphasized by a dash.

to show that the covariance function of the refractive index is

$$B_n(R) = 0.31C_n^2\kappa_0^{-2/3}(\kappa_0 R)^{1/3}K_{1/3}(\kappa_0 R).$$

(*b*) For large separation distances such that $\kappa_0 R \gg 1$, show that

$$B_n(R) \sim \frac{0.39C_n^2\kappa_0^{-2/3}}{(\kappa_0 R)^{1/6}}e^{-\kappa_0 R}, \quad \kappa_0 R \gg 1.$$

(*c*) For small separation distances such that $\kappa_0 R \ll 1$, show that

$$B_n(R) \sim 0.52C_n^2\kappa_0^{-2/3}, \quad \kappa_0 R \ll 1.$$

(*d*) Use the results in parts (*a*) and (*c*) to develop the refractive-index structure function.

8. Given the outer scale spectrum model

$$\Phi_n(\kappa) = 0.033C_n^2\kappa^{-11/3}\exp(-\kappa^2/\kappa_m^2)[1 - \exp(-\kappa^2/\kappa_0^2)],$$

(*a*) find the structure function and show, that as $\kappa_m \to \infty$, it becomes

$$D_n(R) = C_n^2R^{2/3} - 1.68C_n^2\kappa_0^{-2/3}\left[{}_1F_1\left(-\frac{1}{3};\frac{3}{2};\ -\frac{\kappa_0^2R^2}{4}\right) - 1\right].$$

(*b*) For $\kappa_0 R \gg 1$, show that the answer in (*a*) reduces to

$$D_n(R) = 1.68C_n^2\kappa_0^{-2/3}.$$

References

1. A. N. Kolmogorov, "The local structure of turbulence in an incompressible viscous fluid for very large Reynolds numbers," *C. R. (Doki) Acad. Sci. U.S.S.R.* **30**, 301–305 (1941).
2. L. F. Richardson, *Weather Prediction by Numerical Process* (Cambridge University Press, Cambridge, U.K., 1922).
3. J. Barat, "Some characteristics of clear-air turbulence in the middle stratosphere," *J. Atmos. Sci.* **39**, 2553–2564 (1982).
4. W. K. Hocking, "Measurements of turbulent energy dissipation rates in the middle atmosphere by radar techniques: A review," *Radio Sci.* **20**, 1403–1422 (1985).
5. H. Tennekes and J. L. Lumley, *A First Course in Turbulence* (MIT Press, Cambridge, MA, 1972).
6. V. I. Tatarskii, *The Effects of the Turbulent Atmosphere on Wave Propagation* (trans. for NOAA by Israel Program for Scientific Translations, Jerusalem, 1971).
7. R. H. Kraichnan, "On Kolmogorov's inertial-range theories," *J. Fluid Mech.* **62**, 305–330 (1974).
8. A. M. Obukhov, "Some specific features of atmospheric turbulence," *J. Fluid Mech.* **13**, 77–81 (1962).
9. A. N. Kolmogorov, "A refinement of previous hypotheses concerning the local structure of turbulence in a viscous incompressible fluid at high Reynolds number," *J. Fluid Mech.* **13**, 82–85 (1962).
10. A. S. Gurvich and A. M. Yaglom, "Breakdown of eddies and probability distribution for small-scale turbulence," *Phys. Fluids Suppl.* **10**, S59–S65 (1967).
11. L. C. Andrews, R. L. Phillips, B. K. Shivamoggi, J. K. Beck, and M. L. Joshi, "A statistical theory for the distribution of energy dissipation in intermittent turbulence," *Phys. Fluids A* **1**, 999–1006 (1989).
12. R. J. Hill and S. F. Clifford, "Modified spectrum of atmospheric temperature fluctuations and its application to optical propagation," *J. Opt. Soc. Am.* **68**, 892–899 (1978).
13. J. C. Owens, "Optical refractive index of air: Dependence on pressure, temperature and compositions," *Appl. Opt.* **6**, 51–59 (1967).
14. R. J. Hill and G. R. Ochs, "Inner-scale dependence of scintillation variances measured in weak scintillation," *J. Opt. Soc. Am. A* **9**, 1406–1411 (1992).
15. E. A. Novikov, "The energy spectrum of incompressible turbulent flow," *Dokl. Akad. Nauk. SSSR* **139**, 331–333 (1961).
16. A. M. Obukhov, "Structure of the temperature field in turbulent flow," *Izv. Akad. Nauk. SSSR*, Ser. Geogr. I Geofiz. **13**, 58–69 (1949).
17. S. Corrsin, "On the spectrum of isotropic temperature fluctuations in isotropic turbulence," *J. Appl. Phys.* **22**, 469–473 (1951).
18. F. H. Champagne, C. A. Friehe, J. C. LaRue, and J. C. Wyngaard, "Flux measurements, flux-estimation techniques, and fine-scale turbulence

measurements in the unstable surface layer over land," *J. Atmosp. Sci.* **34**, 515–530 (1977).
19. R. M. Williams and C. A. Paulson, "Microscale temperature and velocity spectra in the atmospheric boundary layer boundary layer," *J. Fluid Mech.* **83**, 547–567 (1977).
20. R. J. Hill, "Models of the scalar spectrum for turbulent advection," *J. Fluid Mech.* **88**, 541–662 (1978).
21. M. M. Dubovikov and V. I. Tatarskii, "Calculation of the asymptotic form of the spectrum of locally isotropic turbulence in the viscous range," *Sov. Phys. JEPT* **66**, 1136–1141 (1987).
22. V. I. Tatarskii, M. M. Dubovikov, A. A. Praskovshy, and M. Yu. Karyakin, "Temperature fluctuation spectrum in the dissipation range for statistically isotropic turbulent flow," *J. Fluid Mech.* **238**, 683–697 (1991).
23. L. C. Andrews, "An analytical model for the refractive index power spectrum and its application to optical scintillations in the atmosphere," *J. Mod. Opt.* **39**, 1849–1853 (1992).
24. J. H. Churnside, "A spectrum of refractive-index turbulence in the turbulent atmosphere," *J. Mod. Opt.* **37**, 13–16 (1990).
25. R. Frehlich, "Laser scintillation measurements of the temperature spectrum in the atmospheric surface layer," *J. Atmos. Sci.* **49**, 1494–1509 (1992).
26. L. C. Andrews, *Special Functions of Mathematics for Engineers*, 2nd ed. (SPIE Optical Engineering Press, Bellingham, Wash.; Oxford University Press, Oxford, 1998); [formerly published as 2nd ed. by McGraw-Hill, New York (1992)].
27. L. R. Tsvang, "Microstructure of temperature fields in the free atmosphere," *Radio Sci.* **4**, 1175–1177 (1969).
28. D. L. Fried, "Remote probing of the optical strength of atmospheric turbulence and of wind velocity," *Proc. IEEE* **57**, 415–420 (1969).
29. J. W. Strohbehn, "Remote sensing of clear-air turbulence," *J. Opt. Soc. Am.* **60**, 948 (1970).
30. R. S. Lawrence, G. R. Ochs, and S. F. Clifford, "Measurements of atmospheric turbulence relevant to optical propagation," *J. Opt. Soc. Am.* **60**, 826–830 (1970).
31. J. L. Bufton, P. O. Minott, and M. W. Fitzmaurice, "Measurements of turbulence profiles in the troposphere," *J. Opt. Soc. Am.* **62**, 1068–1070 (1972).
32. D. W. Beran, W. H. Hooke, and S. F. Clifford, "Acoustic echo-sounding techniques and their application to gravity-wave, turbulence, and stability studies," *Boundary-Layer Meterol.* **4**, 133–153 (1973).
33. M. Fukushima, K. Akita, and H. Tanaka, "Night-time profiles of temperature fluctuations deduced from two-year solar observation," *J. Meterol. Soc. Jpn.* **53**, 487–491 (1975).
34. G. R. Ochs, T. Wang, R. S. Lawrence, and S. F. Clifford, "Refractive turbulence profiles measured by one-dimensional spatial filtering of scintillations," *Appl. Opt.* **15**, 2504–2510 (1976).

35. T. E. VanZandt, J. L. Green, K. S. Gage, and W. L. Clark, "Vertical profiles of refractivity turbulence structure constant: comparison of observations by the sunset radar with a new theoretical model," *Radio Sci.* **13**, 819–829 (1978).
36. R. B. Chadwick and K. P. Moran, "Long-term measurements of C_n^2 in the boundary layer," *Radio Sci.* **15**, 355–361 (1980).
37. F. W. Eaton, W. A. Peterson, J. R. Hines, K. R. Peterman, R. E. Good, R. R. Beland, and J. W. Brown, "Comparisons of VHF radar, optical, and temperature fluctuation measurements of C_n^2, r_0, and Θ_0," *Theor. Appl. Climatol.* **39**, 17–29 (1988).
38. F. Dalaudier, M. Crochet, and C. Sidi, "Direct comparison between in situ and radar measurements of temperature fluctuation spectra: a puzzling result," *Radio Sci.* **24**, 311–324 (1989).
39. R. R. Beland, "Propagation through atmospheric optical turbulence," in *The Infrared and ElectroOptical Systems Handbook*, F. G. Smith, ed. (SPIE Optical Engineering Press, Bellingham, Wash., 1993), Vol. 2, Chap. 2.
40. W. W. Brown, M. C. Roggeman, T. J. Schultz, T. C. Havens, J. T. Beyer, and L. J. Otten, "Measurement and data-processing approach for estimating the spatial statistics of turbulence-induced index of refraction fluctuations in the upper atmosphere," *Appl. Opt.* **40**, 1863–1871 (2001).
41. J. T. Beyer, M. C. Roggeman, L. J. Otten, T. J. Schultz, T. C. Havens, and W. W. Brown, "Experimental estimation of the spatial statistics of turbulence-induced index of refraction fluctuations in the upper atmosphere," *Appl. Opt.* **42**, 908–921 (2003).